REFERENCES AND NOTES

1. National Renewable Energy Laboratory, *Best Research-Cell Efficiencies*, www.nrel.gov/pv/assets/images/efficiency_chart.jpg (2016).
2. D. P. McMeekin *et al.*, *Science* **351**, 151–155 (2016).
3. N. K. Noel *et al.*, *Energy Environ. Sci.* **7**, 3061–3068 (2014).
4. F. Hao *et al.*, *J. Am. Chem. Soc.* **137**, 11445–11452 (2015).
5. F. Hao, C. C. Stoumpos, R. P. H. Chang, M. G. Kanatzidis, *J. Am. Chem. Soc.* **136**, 8094–8099 (2014).
6. L. Zhu *et al.*, *Nanoscale* **8**, 7621–7630 (2016).
7. Z. Yang *et al.*, *Adv. Mater.* 10.1002/adma.201602696 (2016).
8. Y. Zhou *et al.*, *J. Mater. Chem. A Mater. Energy Sustain.* **3**, 8178–8184 (2015).
9. See supplementary materials on *Science* Online.
10. C. C. Stoumpos, C. D. Malliakas, M. G. Kanatzidis, *Inorg. Chem.* **52**, 9019–9038 (2013).
11. J. Im, C. C. Stoumpos, H. Jin, A. J. Freeman, M. G. Kanatzidis, *J. Phys. Chem. Lett.* **6**, 3503–3509 (2015).
12. L. M. Herz, *Annu. Rev. Phys. Chem.* **67**, 65–89 (2016).
13. W. Rehman *et al.*, *Adv. Mater.* **27**, 7938–7944 (2015).
14. E. S. Parrott *et al.*, *J. Phys. Chem. Lett.* **7**, 1321–1326 (2016).
15. M. B. Johnston, L. M. Herz, *Acc. Chem. Res.* **49**, 146–154 (2016).
16. P. Docampo, J. M. Ball, M. Darwich, G. E. Eperon, H. J. Snaith, *Nat. Commun.* **4**, 2761 (2013).
17. Z. Li *et al.*, *Chem. Mater.* **28**, 284–292 (2016).
18. J.-W. Lee *et al.*, *Adv. Energy Mater.* **5**, 1501310 (2015).
19. C. Yi *et al.*, *Energy Environ. Sci.* **9**, 656–662 (2016).
20. T. K. Todorov, O. Gunawan, T. Gokmen, D. B. Mitzi, *Prog. Photovolt. Res. Appl.* **21**, 82–87 (2013).
21. P. Schulz *et al.*, *Energy Environ. Sci.* **7**, 1377–1381 (2014).
22. C. Wang *et al.*, *Appl. Phys. Lett.* **106**, 111603 (2015).
23. H. J. Snaith, *Adv. Funct. Mater.* **20**, 13–19 (2010).
24. M. A. Green, K. Emery, Y. Hishikawa, W. Warta, E. D. Dunlop, *Prog. Photovolt. Res. Appl.* **23**, 1–9 (2015).
25. F. Hao, C. C. Stoumpos, D. H. Cao, R. P. H. Chang, M. G. Kanatzidis, *Nat. Photonics* **8**, 489–494 (2014).
26. T. Leijtens *et al.*, *Adv. Energy Mater.* **5**, 1500963 (2015).
27. B. Conings *et al.*, *Adv. Energy Mater.* **5**, 1500477 (2015).
28. M. Saliba *et al.*, *Science* **354**, 206–209 (2016).
29. K. A. Bush *et al.*, *Adv. Mater.* **28**, 3937–3943 (2016).
30. J. Werner *et al.*, *J. Phys. Chem. Lett.* **7**, 161–166 (2016).
31. S. Albrecht *et al.*, *Energy Environ. Sci.* **9**, 81–88 (2015).
32. A. Hadipour *et al.*, *Adv. Funct. Mater.* **16**, 1897–1903 (2006).

ACKNOWLEDGMENTS

We thank M. T. Hörantner for performing the Shockley-Queisser calculation. The research leading to these results has received funding from the Graphene Flagship (Horizon 2020 grant no. 696656 - GrapheneCore1), the Leverhulme Trust (grant RL-2012-001), the UK Engineering and Physical Sciences Research Council (grant EP/J009857/1 and EP/M020517/1), and the European Union Seventh Framework Programme (FP7/2007-2013) under grant agreement nos. 239578 (ALIGN) and 604032 (MESO). T.L. is funded by a Marie Sklodowska Curie International Fellowship under grant agreement H2O2IF-GA-2015-659225. A.B. is financed by IMEC (Leuven) in the framework of a joint Ph.D. program with Hasselt University. B.C. is a postdoctoral research fellow of the Research Fund Flanders (FWO). We also acknowledge the U.S. Office of Naval Research for support. We acknowledge the use of the University of Oxford Advanced Research Computing (ARC) facility (http://dx.doi.org/10.5281/zenodo.22558) and the ARCHER UK National Super-computing Service under the "AMSEC" Leadership project. We thank the Global Climate and Energy Project (GCEP) at Stanford University. All data pertaining to the conclusions of this work can be found in the main paper and the supplementary materials.

SUPPLEMENTARY MATERIALS

www.sciencemag.org/content/354/6314/861/suppl/DC1
Materials and Methods
Supplementary Text
Figs. S1 to S21
Tables S1 and S2
References (*33*–*43*)

27 April 2016; resubmitted 15 August 2016
Accepted 4 October 2016
Published online 20 October 2016
10.1126/science.aaf9717

ORGANIC CHEMISTRY

Asymmetric synthesis of batrachotoxin: Enantiomeric toxins show functional divergence against Na_V

Matthew M. Logan,* Tatsuya Toma,† Rhiannon Thomas-Tran,‡ J. Du Bois§

The steroidal neurotoxin (−)-batrachotoxin functions as a potent agonist of voltage-gated sodium ion channels (Na_Vs). Here we report concise asymmetric syntheses of the natural (−) and non-natural (+) antipodes of batrachotoxin, as well both enantiomers of a C-20 benzoate–modified derivative. Electrophysiological characterization of these molecules against Na_V subtypes establishes the non-natural toxin enantiomer as a reversible antagonist of channel function, markedly different in activity from (−)-batrachotoxin. Protein mutagenesis experiments implicate a shared binding side for the enantiomers in the inner pore cavity of Na_V. These findings motivate and enable subsequent studies aimed at revealing how small molecules that target the channel inner pore modulate Na_V dynamics.

The phenotypic effects of acute poisons found among the rich pharmacopeia of terrestrial and marine life have been documented from antiquity. Isolation and characterization of toxic compounds have made available important chemical reagents for studying complex biochemical circuits (*1*). Studies of this type have revealed a large number of peptide and small-molecule agents that target voltage-gated sodium ion channels (Na_Vs), an obligatory class of membrane proteins for bioelectrical signaling (*1*–*4*). Among the collection of known Na_V modulators are three structurally related agents, (−)-batrachotoxin [(−)-BTX], veratridine, and aconitine (Fig. 1A)—sterically large, lipophilic amine derivatives believed to share a common binding locus in the inner pore region of Na_V (*3*) (site 2, Fig. 1B). The influence of these toxins on ion gating, however, differs distinctly. On one extreme, (−)-BTX, the primary toxic constituent of Colombian poison dart frogs (genus *Phyllobates*), is a full Na_V agonist, causing the channel to open more readily at hyperpolarized membrane potentials and blocking fast inactivation (among other characteristic effects) (*3*–*5*). Conversely, the activities of veratridine and aconitine are best described as partial agonism and inhibition of channel function, respectively (*5*). Despite recent insights from structural biology into the three-dimensional architecture of prokaryotic Na_Vs (*6*–*9*), a molecular understanding of the influence of the site 2 toxins on ion conduction and ion gating kinetics is lacking. Toxin structure-activity studies, in combination with protein mutagenesis experiments, can address questions related to the dynamical nature of channel function and may guide the rational design of small-molecule modulators of Na_V activity (*1*). The potency of (−)-BTX (*10*), its storied history as the archetypal small-molecule site 2 probe (*4*), and its unparalleled effects on channel gating render it an optimal "lead" compound for such investigations.

(−)-BTX binding to Na_Vs alters every aspect of channel function, resulting in a hyperpolarized shift in the voltage dependence of activation, inhibition of both fast and slow inactivation, a decrease in single-channel conductance, and reduction of ion selectivity (*3*, *4*). The utility of this natural product as a Na_V activator has led to a substantial depletion in the world supply, which once exceeded 1 g but was less than 170 mg as of 2009 (*11*, *12*). Since the toxin was first isolated in 1963 by Märki and Witkop from poisonous frogs collected in the northern rain forest of Colombia (*13*), *Phyllobates* has been placed on the endangered species list, and thus collection of natural (−)-BTX from this source is restricted. (−)-BTX has also been identified in select species of birds (genus *Pitohui* and *Ifrita*) (*14*) and beetles (genus *Choresine*) (*15*), but only in small quantities (e.g., ~1.8 μg of (−)-BTX per beetle). Although semi- (*16*) and racemic syntheses (*17*) of BTX-A (Fig. 1C), a compound lacking the C-20 pyrrole ester, have been disclosed, the length of each of these works (>45 linear steps) precludes the facile production of (−)-BTX or select analogs. Accordingly, our desire to use BTX and modified forms thereof for examining channel dynamics and ion gating mechanisms has motivated our efforts to obtain the natural product through de novo synthesis.

Retrosynthetic analysis of (−)-BTX led us to outline a plan that would enable late-stage assembly of the homomorpholine E ring and elaboration of the C-20 allylic ester (Fig. 1C), thereby facilitating access to modified forms of the toxin. Previous structure-activity relationship studies using a small number of semisynthetic BTX derivatives (*10*, *18*) and C/D/E-ring BTX analogs (*19*) revealed the importance of the C-20 ester, tertiary amine, and tetracyclic skeleton for Na_V

Department of Chemistry, Stanford University, Stanford, CA 94305-5080, USA.
*Present address: Gilead Sciences, Foster City, CA 94404, USA.
†Present address: Graduate School of Pharmaceutical Sciences, Nagoya University, Furo-cho, Chikusa-ku, Nagoya 464-8601, Japan.
‡Present address: Arcus Biosciences, Hayward, CA 94545, USA.
§Corresponding author. Email: jdubois@stanford.edu

agonist activity. Unraveling BTX-A exposes a steroid-like frame **1**, the assembly of which is confounded by two angular groups at C/D-ring junction, the C-11 *exo*-methylene and the C-8/C-9 alkene. To maximize convergence in our synthetic plan, we conceived a disconnection strategy for **1** across the C ring. This idea would reduce the problem of constructing **1** into two fragments, one expressing the A/B-ring system (*3*, *20*) and a second comprising the D-ring cyclopentane (*4*, *21*). The successful execution of this scheme could produce the desired toxin through a sequence of linear steps totaling no more than 20 to 25.

Our synthesis of (−)-BTX commenced with the coupling of methylenecyclopentanone **4** (*21*) (fig. S1A) and vinyl bromide **3**, accessed from (*S*)-(+)-Hajos-Parrish ketone through a modified sequence of steps originally outlined by Parsons and co-workers (*20*) (fig. S1B). Conjoining fragments **3** and **4** to generate the linked A/B/D-tricycle **5** presented the first in a series of process development challenges. An initial attempt to effect this transformation involved Li-Br exchange of **3** with *n*-BuLi (Bu, butyl) and sequential addition of enone **4**. Although **5** was delivered under these conditions, product yields never exceeded 30%. Deuterium quenching experiments with D_2O validated our hypothesis that α-deprotonation of **4** was competitive with the desired ketone addition pathway. Transmetalation reactions of the vinyl-lithium species with $ZnCl_2$, $ZnBr_2$, $MgBr_2{\bullet}OEt_2$ (Et, ethyl), $CeCl_3$, $Yb(OTf)_3$ (Tf, trifluoromethansulfonate), $CeCl_3{\bullet}2LiCl$, and $LaCl_3{\bullet}2LiCl$ were examined, but none of these measures proved effective (*22*, *23*). The addition of one equivalent of anhydrous LiBr to the reaction media of **3** improved the coupling efficiency by >20% (*24*). Following this lead, an optimized protocol using 2.1 equivalents of *t*-BuLi, which presumably generates one equivalent of LiBr in situ, reproducibly afforded **5** as a single diastereomer in 65% yield on a multigram scale. The ease of synthesis of this material and its desilylated form **6** enabled subsequent efforts to identify conditions for tandem annulation of the C ring and installation of the quaternary C-13 center.

An evaluation of available methods for ring closure of 1,6-enynes led us to consider radical-initiated processes (*25*). Under such conditions, an incipient C-13 3° radical could be intercepted to forge the angular aminomethylene unit (or a suitable surrogate). Efforts to first examine C-ring formation on **6**, however, revealed the potential fallacy of this plan. Using *n*-Bu_3SnH and triethylborane (Et_3B) to promote the cyclization event resulted in the generation of two isomers, **7** and **8**, in a 1:5 ratio favoring the undesired product (Fig. 2A). Studies by Stork and Beckwith and co-workers have demonstrated that substrate concentration and reaction temperature can influence the mode of cyclization (i.e., 5-*exo*-trig versus 6-*endo*-trig) in radical-mediated enyne reactions (*26*, *27*). At elevated temperature (130°C) and with fivefold dilution of **6**, a reversal in selectivity was observed, affording a slight excess of the desired tetracycle (1.3:1 ratio of **7** to **8**; Fig. 2A). The combined product yield of this transformation exceeded 90%, thus encouraging further exploration of this chemistry, despite the modest selectivity results.

Repeated attempts to capture the intermediate C-13 radical with oxime and hydrazone derivatives generated from formaldehyde failed to deliver the expected aminomethylation product (*28*). Forced to consider alternative solutions, we recognized that a modified silyl ether group appended from the neighboring C-14 alcohol would be aptly positioned to intercept the 3° radical (*29*). Based on available precedent, an alkynylsilyl chloride, $Me_3SiC{\equiv}CSiEt_2Cl$ (Me, methyl), was selected for modification of the C-14 alcohol in **6** (*30*, Fig. 2A). Treatment of the resulting silylether (**9**) with *n*-Bu_3SnH and Et_3B at 150°C resulted in a cyclization cascade to give pentacycle **10** as the exclusive product (*31*). Within the limits of proton nuclear magnetic resonance (^1H NMR) detection, none of the corresponding five-membered C-ring isomer was generated in this process. Our preliminary efforts to understand the role of C-14 substituent groups on reaction selectivity suggest that silyl protection of the alcohol (along with the elevated reaction temperatures) favors 6-*endo*-trig ring closure. Although additional studies are warranted to appreciate these structure-selectivity data, our enyne cyclization cascade offers a convergent approach for synthesizing substituted steroid scaffolds and should facilitate access to a wide range of such compounds.

Close inspection of the radical cyclization products derived from either **6** or **9** revealed an unexpected outcome pertaining to the structure of the resulting organostannane moiety (Fig. 2, A and B). Carbostannylation of the alkyne group should afford a vinyl-tin product, as noted in the reaction of **6**. Unexpectedly, when **9** was subjected to the reaction conditions, allylstannane **10** was the sole product, a result confirmed by both NMR and x-ray crystallography. Formation of allylstannane **10** can be rationalized through a mechanism involving 1,4-H-atom transfer of an intermediate vinyl radical (*32*) (Fig. 2B), a proposal supported by a deuterium labeling experiment (fig. S5). Although this result was unplanned, the efficiency and selectivity of the cyclization reaction compelled our decision to advance this material. Looking forward, the versatility of the allylstannane group should serve future efforts to prepare C ring–modified BTXs.

The availability of **10** in nine steps from the Hajos-Parrish ketone enabled the production of

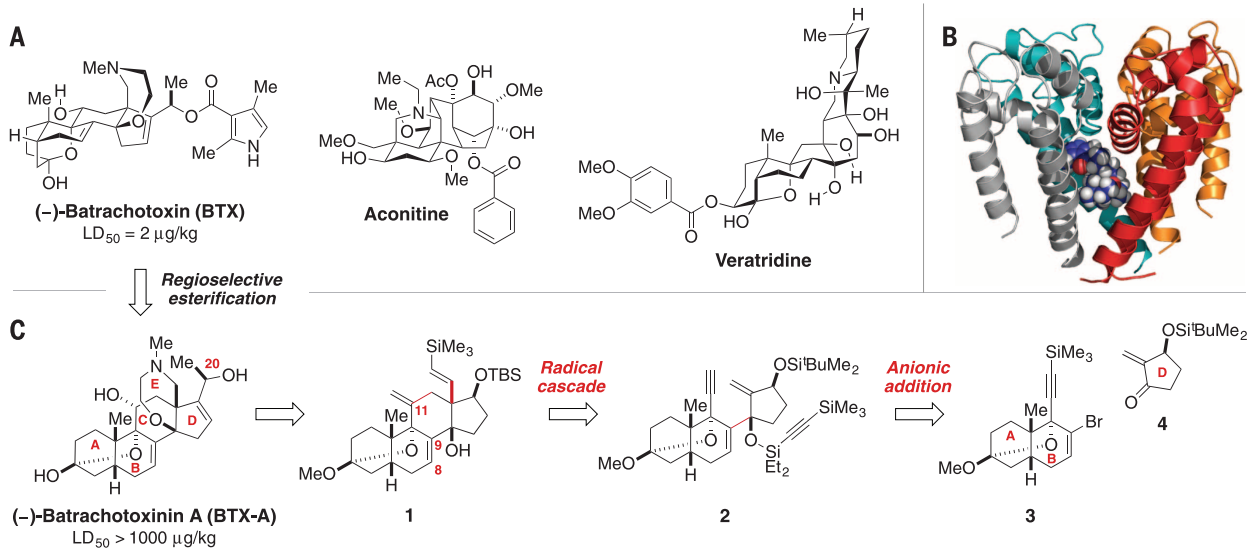

Fig. 1. Background and synthetic plan. (**A**) The structures of lipophilic site 2 toxins (−)-batrachotoxin (BTX), aconitine, and veratridine. (**B**) A pore model of Na_V with (−)-BTX (depicted as spheres) docked at site 2. The structure is based on *Magnetococcus marinus* Na_V crystallographic data (Protein Data Bank accession code 4F4L) (*9*, *19*). Domain I, orange; domain II, red; domain III, gray; domain IV, teal. (**C**) Retrosynthetic analysis of BTX and BTX C-20 ester analogs. LD_{50}, half-maximal lethal dose; Me, methyl; ^{t}Bu, *tert*-butyl; Et, ethyl; TBS, *tert*-butyldimethylsilyl.

substantial quantities of material to complete the target synthesis. Excision of the bridging silyl ether in **10** was accomplished with excess *n*-Bu_4NF, revealing a diol intermediate that was subsequently advanced to **11** through 2-iodoxybenzoic acid–mediated alcohol oxidation and chemoselective vinylsilane cleavage (57%; Fig. 2B). Conversion of aldehyde **11** to chloroacetamide **12** was performed by following a three-step, single-flask sequence (*16*, *33*). From **12,** efficient closure of the homomorpholinamide ring with NaOEt (92%) (*17*) provided a versatile intermediate for modification of both the C- and D-ring units. The latter could be achieved through the D-ring enol triflate, prepared using $KN(SiMe_3)_2$ and $PhNTf_2$.

Introduction of the C-11α alcohol from the C-ring allylstannane **13** presented one of the more difficult challenges in our approach to BTX (Fig. 2B). Although protodestannylation of **13** to generate the corresponding C-11 *exo*-methylenecyclohexane had limited success (*34*), all subsequent attempts to oxidize this compound to ketone **15** (i.e., O_3, OsO_4, and RuO_4) failed to give product. Inspired by a report from Kim and Fuchs, we attempted to convert **13** to the corresponding allyl chloride by using $CuCl_2$ (*35*). Fortuitously, conducting this reaction in dioxane under aerobic conditions delivered enal **14** in 85% yield with only a minor amount of the chlorinated product (~10%). Although the mechanistic details of this transformation remain unclear, we are aware of only one other documented example of such an oxidation reaction, which uses a vanadium catalyst and O_2 (*36*). Enal **14** is suitably disposed for conversion to C-11 ketone **15** by following a series of functional group interconversion steps highlighted by a Curtius rearrangement (*37*). The absence of a viable chromophore on batrachotoxinin A (BTX-A) makes purification of this material difficult; accordingly, in the sequence leading to **15**, the C-3 methoxy acetal was exchanged with *p*-methoxyphenethyl alcohol.

Completion of the carbon skeleton of (–)-BTX was accomplished through a palladium-catalyzed cross-coupling of tributyl(1-ethoxyvinyl)tin to vinyl triflate **15** (Fig. 3A) (*38*). In situ hydrolysis of the incipient enol ether with 1 M oxalic acid supplied enone **16** (77%). Following an extensive screen of reducing agents, successful stereoselective global reduction of enone **16** was accomplished in 33% yield by treatment with freshly prepared AlH_3 (*39*). We hypothesize that the Lewis-basic lactam (or a reduced form) acts as a pivotal stereocontrolling element, as treatment of enone **15** with alternative hydride reducing agents [e.g., AlH_3•NMe_2Et, $NaBH_4$, NH_3•BH_3, (*S*)-Me-CBS-oxazaborolidine/BH_3, or L-selectride] delivered the undesired C-11β alcohol exclusively. The use of AlH_3 also favored generation of the correct C-20 allylic alcohol epimer, a sterochemical outcome that can be rationalized through a model invoking chelation control (*38*). Deprotection of the product from AlH_3 reduction under acidic conditions afforded (–)-BTX-A in 83% yield (*17*). Finally, by employing a modification of Tokuyama, Daly, and Witkop's (–)-BTX-A acylation protocol with the mixed anhydride prepared from ethyl chloroformate and 2,4-dimethyl-pyrrole-3-carboxylic acid (*10*), the synthesis of 2 mg of (–)-BTX was completed [79%, 0.25% overall yield, 24 steps from (*S*)-(+)-Hajos-Parish ketone]. The product was identical in all respects [as assessed by high-resolution mass spectrometry, thin-layer chromatography, and high-performance liquid chromatography (HPLC) coinjection] with a sample of the natural material and with previously recorded spectroscopic data (*40*, *41*). Our synthetic plan also enabled milligram-scale preparation of the unnatural toxin antipode, (+)-BTX, the known benzoate ester of (–)-BTX-A (BTX-B; Fig. 3B) (*42*, *43*), and the enantiomer of this compound (*ent*-BTX-B).

Electrophysiological characterization of synthetic (–)-BTX and BTX-B against rat $Na_V1.4$ ($rNa_V1.4$) confirmed that the latter also functions as an agonist and is similar in potency to the natural product (fig. S6 and table S12). Previous reports and our own studies indicate that the ester group of BTX-B

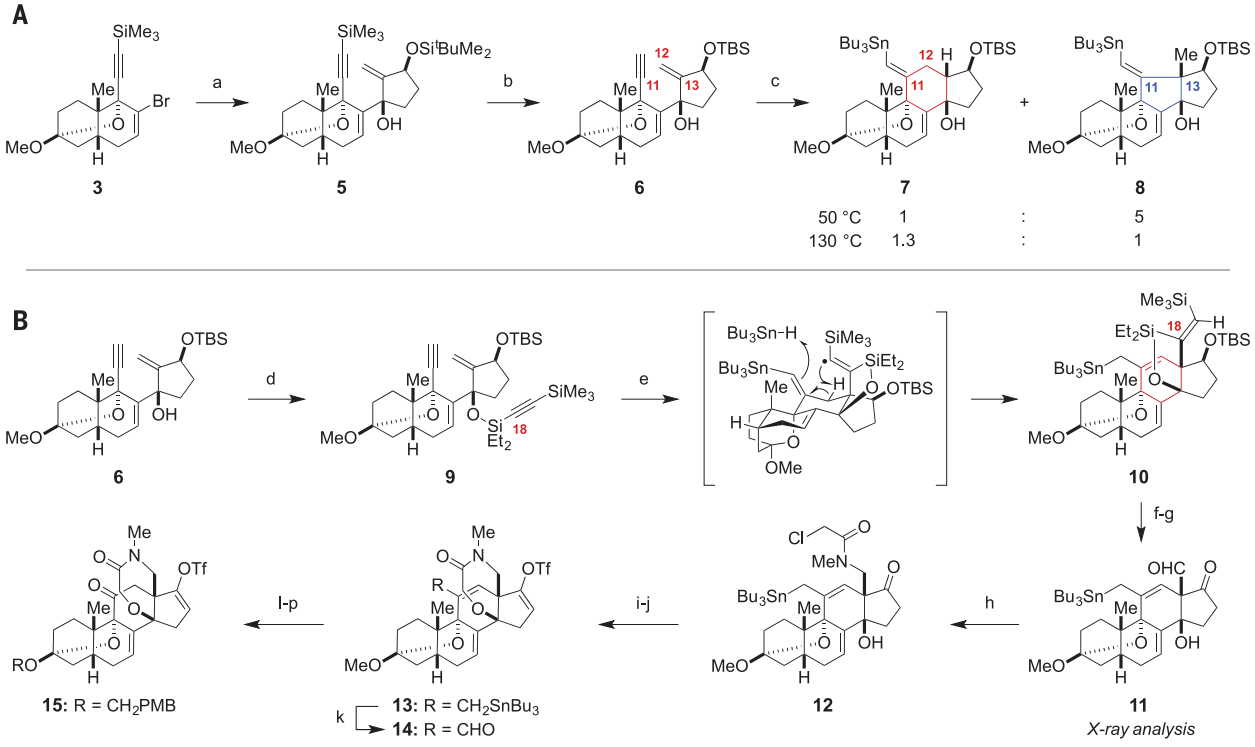

Fig. 2. Enyne radical cyclization to furnish the steroidal core of BTX. Reagents, conditions, and product yields for steps a to p are as follows: (**A**) a, *t*-BuLi, THF, –90°C, then **4** (see Fig. 1) (65%); b, K_2CO_3, MeOH (94%); c, Et_3B, air, *n*-Bu_3SnH. (**B**) d, $Me_3SiC{\equiv}CSiEt_2Cl$, imidazole, CH_2Cl_2 (93%); e, O_2, *n*-Bu_3SnH, Et_3B, Ph_2O, 150°C (75%); f, *n*-Bu_4NF, THF, 60°C (94%); g, 2-iodoxybenzoic acid, *t*-BuOH, 65°C, then OsO_4 [7 mol %], $NaIO_4$, pyridine, H_2O (57%); h, $MeNH_2$, CH_2Cl_2; $NaB(O_2CCF_3)_3H$, CH_2Cl_2, –78°C, then $ClCH_2COCl$, 2,6-lutidine, –78 to 0°C (52%); i, NaOEt, EtOH, 1:1 THF/C_6H_6 (92%); j, $KN(SiMe_3)_2$, $PhNTf_2$, THF, –78 to 0°C (94%); k, $CuCl_2$, O_2, 1,4-dioxane, 73°C (85%); l, $NaClO_2$, NaH_2PO_4, dimethyl sulfoxide/H_2O; m, $SOCl_2$, pyridine, CH_2Cl_2; n, NaN_3, acetone/H_2O; o, aqueous AcOH, 1,4-dioxane, 90°C (57% over four steps); p, *p*-TsOH, 4-Å molecular sieves, *p*-methoxyphenethyl alcohol ($PMBCH_2OH$), C_6H_6 (89%). THF, tetrahydrofuran; Ph, phenyl; Tf, trifluoromethansulfonate; Ts, *p*-toluenesulfonate; Ac, acetate.

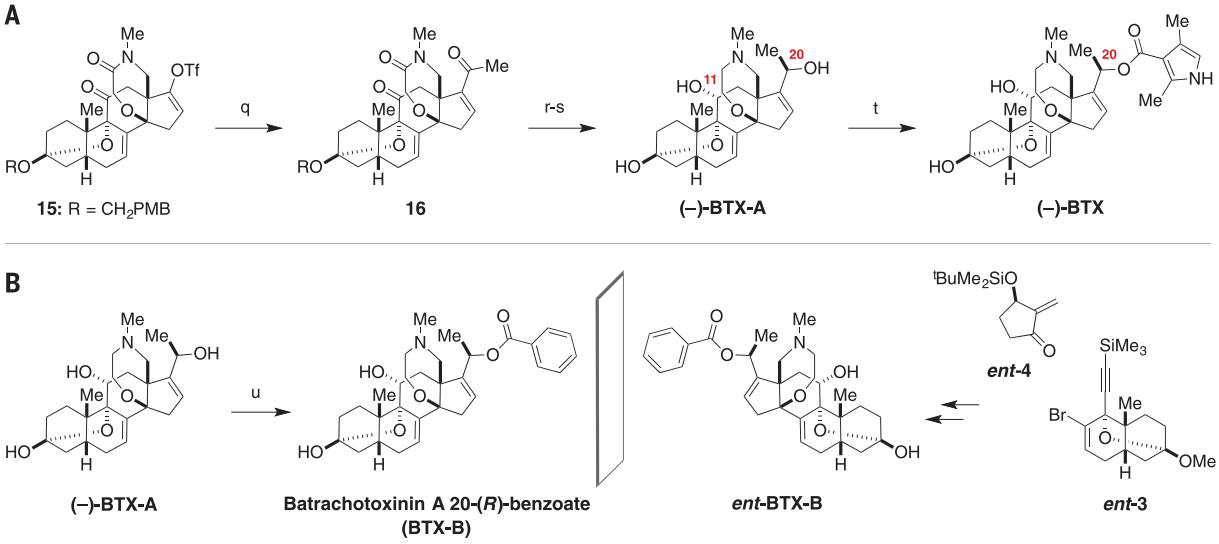

Fig. 3. Completion of the synthesis. Reagents, conditions, and product yields for the preparation of (**A**) (–)-BTX (steps q to t) and (**B**) BTX-B and its enantiomer (steps q to s, then u) are as follows: q, LiCl, CuCl, $Pd(PPh_3)_4$, tributyl(1-ethoxyvinyl)tin, THF, 60°C, then 1 M oxalic acid, 0°C (77%); r, AlH_3, THF, –78 to 0°C (33%); s, *p*-TsOH, 3:2 acetone/H_2O (83%); t, (ethyl carbonic)-2,4-dimethyl-1*H*-pyrrole-3-carboxylic anhydride, Et_3N, C_6H_6, 45°C (79%); u, benzoic (ethyl carbonic) anhydride, Et_3N, C_6H_6, 45°C (70%).

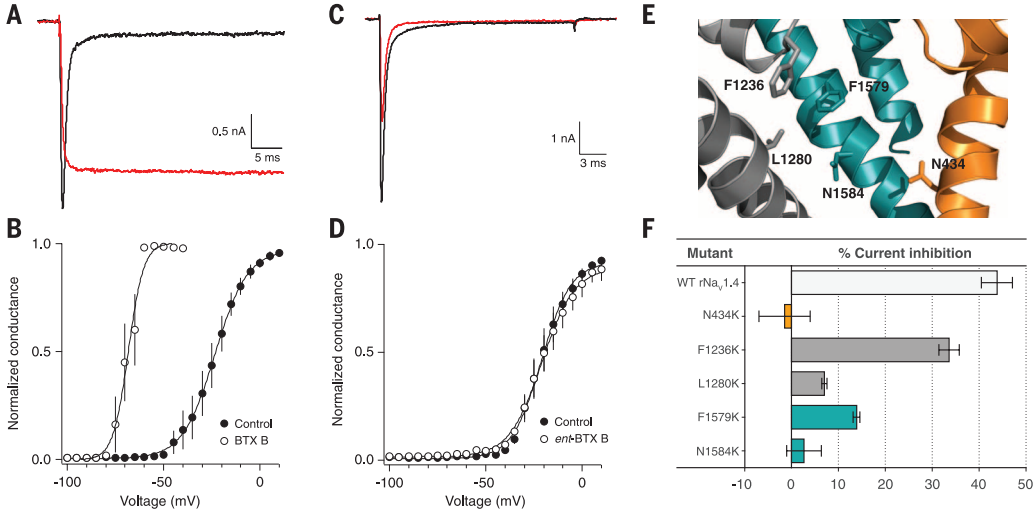

Fig. 4. Effects of synthetic BTX-B and *ent*-BTX-B on wild-type rat $Na_V1.4$ function. (**A**) Representative trace for rat $Na_V1.4$ ($rNa_V1.4$) current before (black) and after (red) steady-state binding of 10 μM BTX-B. Current was evoked by a 150-ms test pulse from –120 to 0 mV after establishment of steady-state inhibition by repetitive depolarizing pulses to 0 mV. (**B**) Voltage dependence of activation for $rNa_V1.4$ in the presence of 10 μM BTX-B (open circles) compared with control conditions (filled circles) for $n \geq 3$ cells (mean ± SD). (**C**) Representative trace for $rNa_V1.4$ current before (black) and after (red) steady-state binding of 5 μM *ent*-BTX-B. Current was evoked by a 24-ms test pulse from –120 to 0 mV after establishment of steady-state inhibition by repetitive depolarizing pulses to 0 mV. (**D**) Voltage dependence of activation for $rNa_V1.4$ in the presence of 10 μM *ent*-BTX-B (open circles) compared with control conditions (filled circles) for $n \geq 3$ cells (mean ± SD). (**E**) $rNa_V1.4$ homology model highlighting residues that have previously been shown to abolish (–)-BTX activity. (**F**) Percent current inhibition of $rNa_V1.4$ mutants by 5 μM *ent*-BTX-B (mean ± SD). WT, wild type; F, phenylalanine; K, lysine; L, leucine; N, asparagine.

is more stable than the oxidatively sensitive acylpyrrole of BTX; thus, additional experiments were performed with the former compound (*42*, *43*). Synthetic BTX-B was tested against a subset of representative Na_V isoforms including $rNa_V1.4$, human $Na_V1.5$, and human $Na_V1.7$. Application of 10 μM BTX-B to Chinese hamster ovary cells expressing a single Na_V subtype resulted in sustained sodium current in all cases (Fig. 4A and figs. S7 and S8). Use-dependent agonism of Na_V isoforms by BTX-B prevented steady-state inactivation of >80% of the sodium channel population (Fig. 4A and fig. S8). BTX-B also induced a characteristic hyperpolarizing shift (–44.9 to –51.5 mV) in the half-maximal voltage ($V_{0.5}$) of activation of wild-type Na_V isoforms (Fig. 4B and table S13). The similarity of these data is consistent with the high protein sequence conservation between Na_V subtypes in the inner pore–lining S6 helices that form the putative toxin binding site (fig. S9).

Following earlier work from our laboratory (*19*) and others (*44*, *45*), we questioned whether the enantiomer form of BTX would bind with high affinity to Na_V with analogous functional effects. Such a question can only be answered with the availability of a de novo synthesis of the toxin. Accordingly, electrophysiological recordings with *ent*-BTX-B were performed against $rNa_V1.4$. These data revealed *ent*-BTX-B to be a use- and state-dependent channel antagonist, with a measured half-maximal inhibitory concentration of 5.3 ± 0.6 μM [Fig. 4C and fig. S10; (+)-BTX also displays antagonistic activity (fig. S11)]. The concentration for half-maximal inhibition of Na_V by *ent*-BTX-B is similar in magnitude to the half-maximal effective concentration for BTX-B agonism (1.0 ± 0.1 μM; fig. S10) measured under identical conditions. Notably, unlike the natural antipode, *ent*-BTX-B binding caused only a minimal shift in the $V_{0.5}$ of activation and the $V_{0.5}$ of steady-state inactivation (table S14). In

addition, channel block was fully reversible by this inhibitor.

To determine whether BTX-B and *ent*-BTX-B share an overlapping binding site within the inner pore region of Na_V, *ent*-BTX-B was tested against five $rNa_V1.4$ single-point mutants that have been shown previously to destabilize BTX binding (Fig. 4, E and F, and fig. S12) (*19*). Mutation of N434 (*46*), L1280 (*47*), F1579 (*48*), and N1584 (*48*) to lysine resulted in a ~3- to 30-fold decrease in current block by 5 μM *ent*-BTX-B. Against F1236K (*49*), however, *ent*-BTX-B retained significant activity (33.6 ± 2.1% current inhibition). The evident difference between *ent*-BTX-B and BTX-B indicates an overlapping, but nonidentical, binding region within the inner pore cavity. It would seem that the open channel is sufficiently large to accommodate lipophilic tertiary amine ligands (*19*, *45*, *50*). Subtle alterations in the binding pose of these ligands appear to dramatically alter the functional response of the protein. Future investigations will be directed at delineating the precise channel-toxin interactions that distinguish activation from inhibition by BTX derivatives and related lipophilic toxins.

REFERENCES AND NOTES

1. M. de Lera Ruiz, R. L. Kraus, *J. Med. Chem.* **58**, 7093–7118 (2015).
2. A. P. Thottumkara, W. H. Parsons, J. Du Bois, *Angew. Chem. Int. Ed. Engl.* **53**, 5760–5784 (2014).
3. S. Y. Wang, G. K. Wang, *Cell. Signal.* **15**, 151–159 (2003).
4. B. I. Khodorov, *Prog. Biophys. Mol. Biol.* **45**, 57–148 (1985).
5. W. A. Catterall, *J. Biol. Chem.* **252**, 8669–8676 (1977).
6. J. Payandeh, T. Scheuer, N. Zheng, W. A. Catterall, *Nature* **475**, 353–358 (2011).
7. J. Payandeh, T. M. Gamal El-Din, T. Scheuer, N. Zheng, W. A. Catterall, *Nature* **486**, 135–139 (2012).
8. X. Zhang *et al.*, *Nature* **486**, 130–134 (2012).
9. E. C. McCusker *et al.*, *Nat. Commun.* **3**, 1102–1110 (2012).
10. T. Tokuyama, J. Daly, B. Witkop, *J. Am. Chem. Soc.* **91**, 3931–3938 (1969).
11. T. Tokuyama, *Heterocycles* **79**, 3–8 (2009).
12. H. M. Garraffo, T. F. Spande, *Heterocycles* **79**, 195–205 (2009).
13. F. Märki, B. Witkop, *Experientia* **19**, 329–338 (1963).
14. J. P. Dumbacher, B. M. Beehler, T. F. Spande, H. M. Garraffo, J. W. Daly, *Science* **258**, 799–801 (1992).
15. J. P. Dumbacher *et al.*, *Proc. Natl. Acad. Sci. U.S.A.* **101**, 15857–15860 (2004).
16. R. Imhof *et al.*, *Helv. Chim. Acta* **55**, 1151–1153 (1972).
17. M. Kurosu, L. R. Marcin, T. J. Grinsteiner, Y. Kishi, *J. Am. Chem. Soc.* **120**, 6627–6628 (1998).
18. B. I. Khodorov *et al.*, *Cell. Mol. Neurobiol.* **12**, 59–81 (1992).
19. T. Toma, M. M. Logan, F. Menard, A. S. Devlin, J. Du Bois, *ACS Chem. Neurosci.* **7**, 1463–1468 (2016).
20. P. Lacrouts, P. J. Parsons, C. S. Penkett, A. R. Raza, *Synlett* **18**, 2767–2768 (2005).
21. S. Takano, T. Yamane, M. Takahashi, K. Ogasawara, *Synlett* **1992**, 410–412 (1992).
22. G. A. Molander, *Chem. Rev.* **92**, 29–68 (1992).
23. A. Krasovskiy, F. Kopp, P. Knochel, *Angew. Chem. Int. Ed. Engl.* **45**, 497–500 (2006).
24. P. E. Van Rijn, S. Mommers, R. G. Visser, H. D. Verkruijsse, L. Brandsma, *Synthesis* **1981**, 459–460 (1981).
25. G. Stork, R. Mook Jr., *J. Am. Chem. Soc.* **109**, 2829–2831 (1987).
26. G. Stork, R. Mook Jr., *Tetrahedron Lett.* **27**, 4529–4532 (1986).
27. A. L. J. Beckwith, D. M. O'Shea, *Tetrahedron Lett.* **27**, 4525–4528 (1986).
28. D. J. Hart, F. L. Seely, *J. Am. Chem. Soc.* **110**, 1631–1633 (1988).
29. G. Stork, H. Suh, G. Kim, *J. Am. Chem. Soc.* **113**, 7054–7056 (1991).
30. R. Bürli, A. Vasella, *Helv. Chim. Acta* **79**, 1159–1168 (1996).
31. K. Nozaki, K. Oshima, K. Utimoto, *J. Am. Chem. Soc.* **109**, 2547–2549 (1987).
32. M. Gulea, J. M. Lopez-Romero, L. Fensterbank, M. Malacria, *Org. Lett.* **2**, 2591–2594 (2000).
33. G. W. Gribble, *Chem. Soc. Rev.* **27**, 395–404 (1998).
34. M. Andrianome, B. Delmond, *J. Chem. Soc. Chem. Commun.* **1985**, 1203–1204 (1985).
35. S. Kim, P. L. Fuchs, *J. Am. Chem. Soc.* **115**, 5934–5940 (1993).
36. T. Hirao, C. Morimoto, T. Takada, H. Sakurai, *Tetrahedron Lett.* **42**, 1961–1963 (2001).
37. R. L. Snowden, S. M. Linder, M. Wüst, *Helv. Chim. Acta* **72**, 892–905 (1989).
38. A. Sloan Devlin, J. Du Bois, *Chem. Sci.* **4**, 1059–1063 (2013).
39. A. I. Meyers, L. E. Burgess, *J. Org. Chem.* **56**, 2294–2296 (1991).
40. A 10-μg sample of authentic (−)-BTX was purchased from Santa Cruz Biotech.
41. T. Tokuyama, J. W. Daly, *Tetrahedron* **39**, 41–47 (1983).
42. G. B. Brown, S. C. Tieszen, J. W. Daly, J. E. Warnick, E. X. Albuquerque, *Cell. Mol. Neurobiol.* **1**, 19–40 (1981).
43. W. A. Catterall, C. S. Morrow, J. W. Daly, G. B. Brown, *J. Biol. Chem.* **256**, 8922–8927 (1981).
44. S. Mehrotra *et al.*, *J. Nat. Prod.* **77**, 2553–2560 (2014).
45. C. Nau, S. Y. Wang, G. R. Strichartz, G. K. Wang, *Mol. Pharmacol.* **56**, 404–413 (1999).
46. S. Y. Wang, G. K. Wang, *Proc. Natl. Acad. Sci. U.S.A.* **95**, 2653–2658 (1998).
47. S. Y. Wang, C. Nau, G. K. Wang, *Biophys. J.* **79**, 1379–1387 (2000).
48. S. Y. Wang, G. K. Wang, *Biophys. J.* **76**, 3141–3149 (1999).
49. S. Y. Wang, J. Mitchell, D. B. Tikhonov, B. S. Zhorov, G. K. Wang, *Mol. Pharmacol.* **69**, 788–795 (2006).
50. B. S. Zhorov, D. B. Tikhonov, *Trends Pharmacol. Sci.* **34**, 154–161 (2013).

ACKNOWLEDGMENTS

We are grateful to M. Maduke (Stanford University) for generous use of her laboratory space and equipment. We thank S. Lynch (Stanford University) for assistance with NMR experiments and analysis, Y. Kishi (Harvard University) for graciously providing NMR spectra of synthetic BTX-A, J. K. Maclaren (Stanford Nano Shared Facilities) for solving the crystal structure of **11** (supported by the NSF under award ECCS-1542152), G. Dick (Stanford University) for assistance with HPLC coinjection of natural and synthetic BTX, and the Vincent Coates Foundation Mass Spectrometry Laboratory, Stanford University Mass Spectrometry (https://mass-spec.stanford.edu). Metrical parameters for the structure of compound **11** are available free of charge from the Cambridge Crystallographic Data Centre under reference number CCDC-1509206. This work was supported in part by the NIH (R01NS045684) and by gifts from Pfizer and Amgen. T.T. was sponsored as a Japan Society for the Promotion of Science Fellow for research abroad. R.T.-T. is a NSF predoctoral fellow. M.M.L. and T.T. contributed to the synthesis of BTX, and R.T.-T. was responsible for electrophysiology experiments. The manuscript was prepared by M.M.L., R.T.-T., and J.D.B. J.D.B. is a cofounder of and owns equity shares in SiteOne Therapeutics, a pharmaceutical startup company aimed at developing sodium channel subtype–selective inhibitors as antinociceptive agents.

SUPPLEMENTARY MATERIALS

www.sciencemag.org/content/354/6314/865/suppl/DC1
Materials and Methods
Figs. S1 to S12
Tables S1 to S14
References (*51*–*58*)

13 June 2016; accepted 14 October 2016
10.1126/science.aag2981

GEOPHYSICS

Coseismic rupturing stopped by Aso volcano during the 2016 M_w 7.1 Kumamoto earthquake, Japan

A. Lin,[1]* T. Satsukawa,[1] M. Wang,[1] Z. Mohammadi Asl,[1] R. Fueta,[1] F. Nakajima[2]

Field investigations and seismic data show that the 16 April 2016 moment magnitude (M_w) 7.1 Kumamoto earthquake produced a ~40-kilometer-long surface rupture zone along the northeast-southwest–striking Hinagu-Futagawa strike-slip fault zone and newly identified faults on the western side of Aso caldera, Kyushu Island, Japan. The coseismic surface ruptures cut Aso caldera, including two volcanic cones inside it, but terminate therein. The data show that northeastward propagation of coseismic rupturing terminated in Aso caldera because of the presence of magma beneath the Aso volcanic cluster. The seismogenic faults of the 2016 Kumamoto earthquake may require reassessment of the volcanic hazard in the vicinity of Aso volcano.

Large earthquakes and active volcanoes are closely related natural phenomena resulting from plate tectonic processes (*1*–*3*). Large earthquakes often accompany or precede volcanic eruptions (*4*, *5*). Seismic analyses and geological observations reveal that the distribution and segmentation of active faults are mainly controlled by the presence of magma bodies in volcanic regions (*6*) and that fault segment boundaries play important roles in a number of aspects of earthquake behavior, including rupture initiation and termination (*7*). Fault segment boundaries generally are associated with a buildup of heterogeneous fault stress (*8*) and large changes in earthquake-induced surface offset (*9*). In volcanic regions, a magma chamber may affect seismicity and the rupture process of an earthquake through the presence of a high-temperature area (*10*), a heterogeneous fault plane on a crater wall (*11*), and/or rectified diffusion (*12*). However, because of a lack of geological data, it is unknown whether a volcano can affect coseismic fault rupturing processes and mechanisms. The 16 April 2016 Kumamoto earthquake of moment magnitude

[1]Department of Geophysics, Graduate School of Science, Kyoto University, Kyoto 606-8502, Japan. [2]CTI Engineering International, Kotou-ku, Tokyo 136-0071, Japan.
*Corresponding author. Email: slin@kugi.kyoto-u.ac.jp

Science

Asymmetric synthesis of batrachotoxin: Enantiomeric toxins show functional divergence against Na_V

Matthew M. Logan, Tatsuya Toma, Rhiannon Thomas-Tran and J. Du Bois

Science **354** (6314), 865-869.
DOI: 10.1126/science.aag2981

Pluses and minuses of BTX behavior

Batrachotoxin is a potent neurotoxin produced by the endangered Colombian poison dart frog and is an agonist of voltage-gated sodium ion channels (NaVs). Logan *et al.* developed a chemical synthesis of this molecule, denoted (–)-BTX, by taking advantage of a tin hydride–mediated radical cyclization to stitch together the polycyclic framework. Using an analogous route, they also prepared the non-natural mirror image, (+)-BTX. Conversely to the natural product, (+)-BTX antagonized NaVs.

Science, this issue p. 865